Pertanika J. Sci. & Technol. 31 (6): 2805 - 2822 (2023)

PERTANIKA JOURNALS

SCIENCE & TECHNOLOGY

Journal homepage: http://www.pertanika.upm.edu.my/

Response Surface Methodology: A Versatile Tool for the Optimization of Particle Sizes of Cellulose Beads

Kimberly Wei Wei Tay[1], Suk Fun Chin[1]*, Mohd Effendi Wasli[1] and Zaki Musa[2]

[1]*Faculty of Resource Science and Technology, Universiti Malaysia Sarawak, 94300 UNIMAS, Kota Samarahan, Sarawak, Malaysia*

[2]*Malaysian Agricultural Research and Development Institute (MARDI), Jalan Santubong, Petra Jaya, 93050 Kuching, Sarawak, Malaysia*

ABSTRACT

Synthesis parameters are of utmost importance for controlling the particle sizes of cellulose beads. This study aims to investigate the effects of synthesis parameters e.g., stirring speed (250–1250 rpm), surfactant concentrations (0.5–6.0% w/v), cellulose concentrations (1–5% w/v), and reaction temperature (30-100°C) on the particle sizes for micron-sized cellulose beads (μCBs) as well as other parameters e.g. the volume (1.0 mL) and concentration (0.1–1.0% w/v) of cellulose for nanosized (*n*CBs) cellulose beads using the response surface methodology (RSM). A total of 27 runs were conducted applying RSM based on the central composite design approach with Minitab-19. Cellulose concentrations were shown to have the most significant effect on both μCBs and *n*CBs. Under optimized conditions, the minimum and maximum mean particle size of μCBs that could be achieved were 15.3 µm and 91 µm, respectively. The predicted mean particle size for *n*CBs was obtained at 0.01 nm as the smallest and 200 nm as the biggest particle size under the optimum conditions. This study envisages that RSM and experiments for targeted applications such as biomedicine and agriculture could optimize the particle sizes of cellulose beads.

Keywords: Cellulose beads, controlled particle sizes, microbeads, nanobeads, response surface methodology

ARTICLE INFO

Article history:
Received: 19 October 2022
Accepted: 25 January 2023
Published: 03 October 2023

DOI: https://doi.org/10.47836/pjst.31.6.10

E-mail addresses:
70097@siswa.unimas.my (Kimberly Wei Wei Tay)
sfchin@unimas.my; sukfunchin@gmail.com (Suk Fun Chin)
wmeffendi@unimas.my (Mohd Effendi Wasli)
zakimusa@mardi.gov.my (Zaki Musa)
* Corresponding author

INTRODUCTION

Cellulose fibers have attracted tremendous interest as a precursor material for the synthesis of micro-beads and nanobeads due to their vast availability, renewability, cost-effectiveness, biocompatibility,

ISSN: 0128-7680
e-ISSN: 2231-8526

biodegradability (Balart et al., 2021; Gericke et al., 2013; Jampi et al., 2021; Kalia et al., 2011; Xu & Cho, 2022). Cellulose fibers can be isolated from various cellulosic wastes such as cotton, sawdust, and printed paper (Pang et al., 2011, 2018; Voon et al., 2016). Cellulose beads in nano and micron sizes have a high potential to be used in various technological and biomedical applications such as solid support, ion exchange, and water treatment (Alazab & Saleh, 2022; Saleh, 2021), protein immobilization (Califano et al., 2021; Culica et al., 2021; Guo et al., 2021) and delayed drug release (Gülsu & Yüksektepe, 2021; Ho et al., 2020; Mohan et al., 2022), slow-release fertilizer (França et al., 2021; Gomes et al., 2022; Machado et al., 2022), dye removal (Hamidon et al., 2022; Harada et al., 2021; Meng et al., 2019) and heavy metal removal (Du et al., 2018; Hu et al., 2018; Liu et al., 2021) due to their versatility and eco-friendliness (Carvalho et al., 2021).

Many researchers have attempted the water in oil microemulsion and nanoprecipitation methods to synthesize μCBs and *n*CBs, respectively. Water in oil (W/O) microemulsion is thermodynamically more stable than oil in water by protecting the water-soluble molecules inside a continuous oil phase (Li et al., 2022; Russell-Jones & Himes, 2011; Song et al., 2020). Surfactant is crucially needed in forming microemulsion (Li et al., 2018). Owing to their adequate cutaneous tolerance, low irritation potential, and less toxicity than anionic surfactants, non-ionic surfactants are preferable, such as sorbitan monooleate, Span 80 as attributed to its biodegradability, biocompatibility, and safe to use in food, cosmetic as well as drug production (Conforti et al., 2021; Lechuga et al., 2016; Roque et al., 2020).

Nanoprecipitation is a straightforward and versatile method that involves the complex interaction between mixing, supersaturation, nucleation, and particle growth (Tay et al., 2012). Thanks to its simplicity and reproducibility, this process is greatly explored to synthesize nanoparticles (Yan et al., 2021). Response surface methodology (RSM) has been widely adopted as it helps achieve optimal conditions with a minimum number of trials (Karri et al., 2018; Sebeia et al., 2021; Shahnaz et al., 2020). Several studies have demonstrated that the RSM method is a very effective and versatile method for determining the effects of multiple synthesis parameters on the morphology and properties of the synthesized products (Allouss et al., 2019; Chin et al., 2021; Jancy et al., 2020; Lee & Patel, 2022; Pal et al., 2022; Wu & Hu, 2021).

The synthesis parameters profoundly affected the particle sizes of the μCBs and *n*CBs (Chin et al., 2018; Voon et al., 2015, 2017b). However, without a proper understanding of the underlying mechanisms between each synthesis parameter and the particle sizes, it is very challenging to precisely and consistently control the particle sizes of the μCBs and *n*CBs. Therefore, a systematic study of the effect of synthesis parameters on the particle sizes for μCBs and *n*CBs by both the experimental method and the RSM is of utmost importance to allow precise control of their particle sizes for targeted applications. In this study, the effects of synthesis parameters on mean particle size for μCBs and *n*CBs were investigated and optimized using the RSM.

MATERIALS AND METHODS

Materials and Reagents

Paper wastes were obtained from Universiti Malaysia Sarawak, particularly on the campus of Faculty Resource and Science Technology. Chemical substances such as sodium dihydrogen phosphate or NaH_2PO_4 (Sigma Aldrich), alpha-cellulose (Sigma Aldrich), as well as disodium hydrogen phosphate or Na_2HPO_4 (Sigma Aldrich) were obtained. Procurement was made for hydrochloric acid or HCl (Merck), sodium hydroxide or NaOH (Merck), urea (Merck), thiourea (Merck), sorbitan oleate or known as Span 80 (Merck), paraffin oil (Merck), absolute ethanol (Merck), as well as sodium dodecyl sulfate or SDS (Merck). No further purification was needed for every chemical applied. Phosphate buffer saline solution, PBS, was prepared using sodium dihydrogen phosphate, NaH_2PO_4 (1.0 M), and disodium hydrogen phosphate, Na_2HPO_4 (1.0 M) solutions. Ultrapure water (~18.2 MΩ·cm, 25°C) was obtained from the Water Purifying System (ELGA, Model Ultra Genetic).

Extraction of Cellulose Fibres

The extraction of cellulose fibers from paper waste was based on our published methods (Voon et al., 2016, 2017a, 2017b). Approximately 100 g of paper waste was turned into powder by grinding and then sprinkled onto the water with constant stirring of 2000 rpm for 2 hours. A treatment with NaOH solution (12.0 wt%) in 24 hours was required for the slurry and, eventually, with HCl solution (3.0 wt%) at 80°C for 2 hours to eliminate hemicellulose, lignin together with residual ink. Refined cellulose fibers were then cleaned with ultrapure water, followed by the drying process in an oven ranging from 60°C to 100˚C for 24 hours to ensure the water content remained below 0.5%. A comparison of the cellulose sample and commercial alpha-cellulose based on the FTIR spectrum was made to confirm the purity of the cellulose sample.

Dissolution of Cellulose

Dissolution of cellulose fibers was conducted by dissolving and sonicating the measured quantity of cellulose fibers in an aqueous-based solvent system, NTU solvent (100 mL) with the composition proportion at 8: 6.5: 8 (% w/v) of NaOH: thiourea: urea respectively for half an hour. The resulting dispersion was cooled by putting it inside a freezer under -20°C for 24 hours to achieve a solid frozen mass and later defrosted at normal room temperature to collect a transparent cellulose solution (Voon et al., 2017a).

Preparation of Cellulose Beads

Fabrication of Micron-sized Cellulose Beads (μCBs). μCBs were synthesized from the cellulose solution by employing the water-in-oil (W/O) microemulsion technique and the

surfactant and precipitating agent, Span 80 and acetic acid, respectively. Span 80 in 0.6 g was commonly dissolved at room temperature in paraffin oil (20 mL). Afterward, half an hour of stirring for the resulting mixture to ensure the homogenized oil phase was attained. Next, microemulsion formation was achieved by adding drop by drop of the cellulose solution (3.5 mL) into the obtained oil phase, along with 1000 rpm of constant stirring for 1 hour. Under vigorous agitation, precipitation of μCBs was observed after incorporating 10% acetic acid. The resulting mixture was used in a separating funnel to obtain cellulose beads and, later, rinsed once with deionized water and two times with absolute ethanol to eliminate the remaining NTU solvent, paraffin oil, and Span 80. The mean particle size of μCBs formed was controlled by modifying the synthesis parameters, which are the stirring speed (250 rpm–1250 rpm), quantity of surfactant (0.5% w/v–6.0% w/v), cellulose concentration (1.0% w/v–5.0% w/v) and reaction temperature (30°C–100°C). Ultimately, μCBs were kept in ethanol (20% v/v) at 0–5°C (Voon et al., 2017a).

Fabrication of Nanosized Cellulose Beads (*n*CBs). The cellulose solution (1 mL) of several concentrations (0.1% w/v–1.0% w/v) was added in a drop-by-drop manner to a specified amount of absolute ethanol (6 mL) just when initiating ultrasonication. Precipitation was seen immediately with a cloudy appearance, indicating the formation of *n*CBs. The obtained suspension was centrifuged. After that, the precipitate was washed five times with absolute ethanol to get rid of the excess NaOH, urea, and thiourea to obtain the *n*CBs (Voon et al., 2017a).

Response Surface Methodology (RSM)

By using Minitab-19 software, a total of 27 runs were made to investigate the effects of synthesis parameters on the mean particle sizes of the μCBs and *n*CBs. Specifically, 22 runs were for μCBs. The p-values for each parameter for both μCBs and *n*CBs are lower than 0.05, as stated in the coded coefficients in Table 1. In addition, the listed p-values in the ANOVA table (Table 2) for the model also provided further validation, deducing that it is statistically significant for all the parameters involved. As shown in Figures 1(a) and (b), the Pareto charts also predicted the same justification. Therefore, the significance of all the synthesis parameters on the mean particle sizes was accurate as estimated by the models applied.

The model's R^2 value and adjusted R^2 (Table 3) for μCBs were estimated to be approximately 92.79% and 88.36%, respectively. As for *n*CBs, the R^2 and adjusted R^2 have the same value of 100%. The evaluation of the goodness of the fit was dependent on statistical parameters like p-value, R^2, and adjusted R^2 (Kim et al., 2020). In this case, these models displayed low p-values, high R^2, and adjusted R^2, indicating that the synthesis parameters used for controlling the particle sizes of the cellulose beads were a good fit with

Table 1
Coded coefficients table of the synthesis parameters for μCBs and nCBs

	Term	Coef	SE Coef	T-Value	P-Value	VIF
*μ*CBs	Constant	35.17	3.72	9.44	0.000*	
	Stirring speed (rpm)	-14.75	2.51	-5.88	0.000*	1.12
	Span 80 concentration (% w/v)	-7.56	2.27	-3.33	0.005*	1.07
	Cellulose concentration (% w/v)	13.32	2.79	4.77	0.000*	1.00
	Temperature (°C)	17.85	2.21	8.07	0.000*	1.62
	SS^2	13.19	4.38	3.01	0.010*	1.10
	SC^2	17.44	3.91	4.46	0.001*	1.10
	CC^2	-2.51	3.46	-0.73	0.481	1.13
	T^2	10.28	3.95	2.60	0.022*	1.59
*n*CBs	Constant	38.23	0.237	161.15	0.004*	
	Cellulose concentration (% w/v)	67.12	0.153	437.51	0.001*	1.75
	VC (mL)	32.90	0.166	197.85	0.003*	2.38
	CC^2	61.79	0.254	243.54	0.003*	1.50

Note. Superscript * refers to the statistically significant parameters ($p < 0.05$). SS^2 represents the squared stirring speed, SC^2 is the squared Span 80 concentration, CC^2 is the squared cellulose concentration, T^2 is the squared temperature, and VC is the volume of cellulose. *μ*CBs involve SS (250–1250 rpm), SC (0.5–6.0% w/v), CC (1–5% w/v), and T (30–100°C), while *n*CBs are VC (1 mL) and CC (0.1–1.0% w/v).

Table 2
Analysis of variance (ANOVA) table for μCBs and nCBs

	Source	DF	Adj SS	Adj MS	F-Value	P-Value
*μ*CBs	Model	8	3261.29	407.66	20.92	0.000*
	Linear	4	2633.13	658.28	33.79	0.000*
	Stirring speed (rpm)	1	674.39	674.39	34.61	0.000*
	Span 80 concentration	1	216.52	216.52	11.11	0.005*
	Cellulose concentration	1	443.56	443.56	22.77	0.000*
	Temperature (°C)	1	1269.51	1269.51	65.16	0.000*
	Square	4	754.90	188.73	9.69	0.001*
	SS^2	1	176.55	176.55	9.06	0.010*
	SC^2	1	387.36	387.36	19.88	0.001*
	CC^2	1	10.27	10.27	0.53	0.481
	T^2	1	131.62	131.62	6.76	0.022*
	Error	13	253.28	19.48		
	Lack-of-Fit	10	175.63	17.56	0.68	0.720
	Pure Error	3	77.65	25.88		
	Total	21	3514.57			
*n*CBs	Model	3	21934.80	7311.60	196270.43	0.002*
	Linear	2	21828.50	10914.20	292979.26	0.001*
	Cellulose concentration (% w/v)	1	7130.60	7130.60	191412.39	0.001*

Table 2 *(continue)*

Source	DF	Adj SS	Adj MS	F-Value	P-Value
VC (mL)	1	1458.30	1458.30	39146.31	0.003*
Square	1	2209.60	2209.60	59313.64	0.003*
CC^2	1	2209.60	2209.60	59313.64	0.003*
Error	1	0.00	0.00		
Total	4	21934.80			

Note. Superscript * refers to the statistically significant parameters ($p < 0.05$). SS^2 represents the squared stirring speed, SC^2 is the squared Span 80 concentration, CC^2 is the squared cellulose concentration, T^2 is the squared temperature, and VC is the volume of cellulose. *μ*CBs involve SS (250–1250 rpm), SC (0.5–6.0% w/v), CC (1–5% w/v), and T (30–100°C), while *n*CBs are VC (1 mL) and CC (0.1–1.0% w/v).

Table 3
Model summary table of the synthesis parameters for μCBs and nCBs

	S	R-sq**	R-sq(adj)**	R-sq(pred)
*μ*CBs	4.41395	92.79%	88.36%	64.17%
*n*CBs	0.19301	100.00%	100.00%	-

Note. ** High values of R-squared and R-squared (adj.) are indicated. *μ*CBs involve SS (250–1250 rpm), SC (0.5–6.0% w/v), CC (1–5% w/v), and T (30–100°C), while *n*CBs are VC (1 mL) and CC (0.1–1.0% w/v).

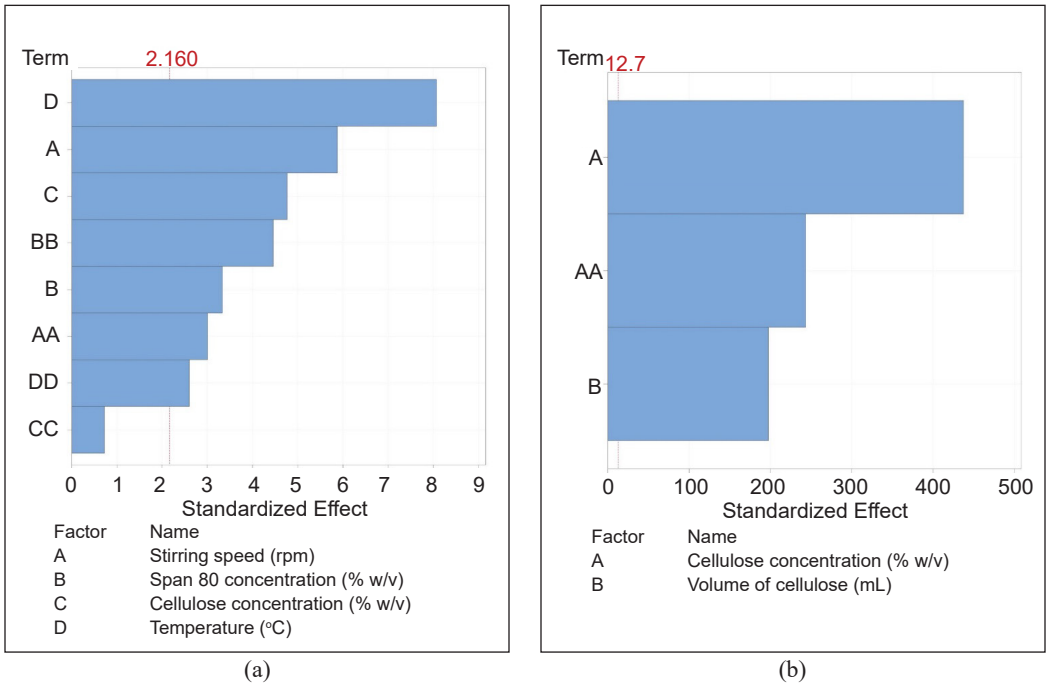

(a) (b)

Figure 1. Pareto charts for the mean particle sizes of (a) *μ*CBs and (b) *n*CBs, where *μ*CBs are SS (250–1250 rpm), SC (0.5–6.0% w/v), CC (1–5% w/v) and T (30–100°C); *n*CBs are VC (1 mL) and CC (0.1–1.0% w/v)

the model. Equations 1 and 2 demonstrated the regression equations in uncoded units of the models for both sized cellulose beads, respectively.

$$\text{Particle sizes } (\mu m) = 96.90 - 0.1086(SS) - 17.74(SC) + 10.43(CC) - 0.581(T) + 0.000053(SS)^2 + 2.306(SC)^2 - 0.629(CC)^2 + 0.00839(T)^2 \quad [1]$$

$$\text{Particle sizes (nm)} = 0.000 - 112.93(CC) + 65.80(VC) + 247.17(CC)^2 \quad [2]$$

Where SS is the stirring speed, SC is the Span 80 concentration, CC is the cellulose concentration, T is temperature, and VC is the volume of cellulose.

RESULTS AND DISCUSSION

Effect of Synthesis Parameters on the Mean Particle Sizes for *μ*CBs

Effects of Stirring Speeds. Figures 2(a) and (b) illustrate the respective contour and surface plots for the effects of stirring speed and Span 80 concentration on the mean particle sizes of *μ*CBs. Both plots anticipated that the minimum mean particle size of 30.2 μm could be attained with a stirring speed of 1023.4 rpm and 3.9% w/v of Span 80 concentration. At the same time, a maximum mean particle size of 87.5 μm was obtained under 254 rpm and 0.5% w/v Span 80 concentration. In our previous study, the smallest 27.6 μm and 64.5 μm particle sizes of *μ*CBs were produced under 1000 rpm and 250 rpm, respectively, with 2% w/v Span 80 (Voon et al., 2017a). A slow stirring speed would decrease the kinetic energy of particles. Eventually, aggregation of particles may tend to occur. Shi et al. (2011) mentioned the difficulty dispersing the cellulose solution in the oil phase under less than 300 rpm stirring speed. The size of the microsphere would also increase under slower stirring (Luo & Zhang, 2010), whereas an increase of 500 rpm stirring speed could lead to a reduction of at least half in the size of cellulose microspheres (Jo et al., 2019; Lefroy et al., 2022) because aggregates would break apart under higher stirring speeds (Kemin & Chin, 2020). As cellulose contains many hydroxyl groups (Shi et al., 2021), the formation of cellulose molecules' intra and intermolecular hydrogen bonds was likely to occur. However, the strong stirring force produced from the high stirring speed might damage the structure of the beads, causing a reduction of compressive strength (Li et al., 2020).

In the presence of surfactants, the interaction of polymer chains would be hindered, forming various reduced mean particle sizes (Tay et al., 2012). Surface tension between particles could be decreased, preventing coalescence from producing smaller particles when applying an optimum surfactant concentration (Chin et al., 2014). For instance, the presence of a carbonyl group would result, as indicated by a strong absorption peak at around 1700 cm^{-1} (Essawy et al., 2016; Guan et al., 2017). It further proved the combination of surfactants with the cellulose and the hindrance of the intermolecular hydrogen bond aggregation of the cellulose due to the exposed hydrophobic polymer chains (Wang et al.,

2019). An increment of surfactant concentration can enhance the micelle formation and lead to a larger mean particle size (Ching et al., 2019; Jo et al., 2019). It has resulted in instability and aggregation of particles, thereby producing larger microspheres (Chin et al., 2014; Hakim et al., 2020). As surfactant concentration increased, the number of micelles also increased, which enhanced the formation of surfactant-polymer complexes via the electrostatic and hydrophobic interactions (Bhardwaj et al., 2018).

However, it had been reported that an increase in surfactant concentrations from 0 % to 3% w/v showed a significant reduction in the particle size of microspheres (Alnaief et al., 2011; Voon et al., 2017a). Specifically, 3% w/v of surfactant concentration was an optimum concentration for fully covering the whole surface area of droplets, providing great stabilization in forming smaller particle sizes (Chin et al., 2014). Therefore, the optimal conditions for forming the smallest mean particle size of beads were approximately 1000 rpm, and within 4% w/v Span 80 concentration could be employed, proving a satisfactory agreement exists between the experimental and predicted results.

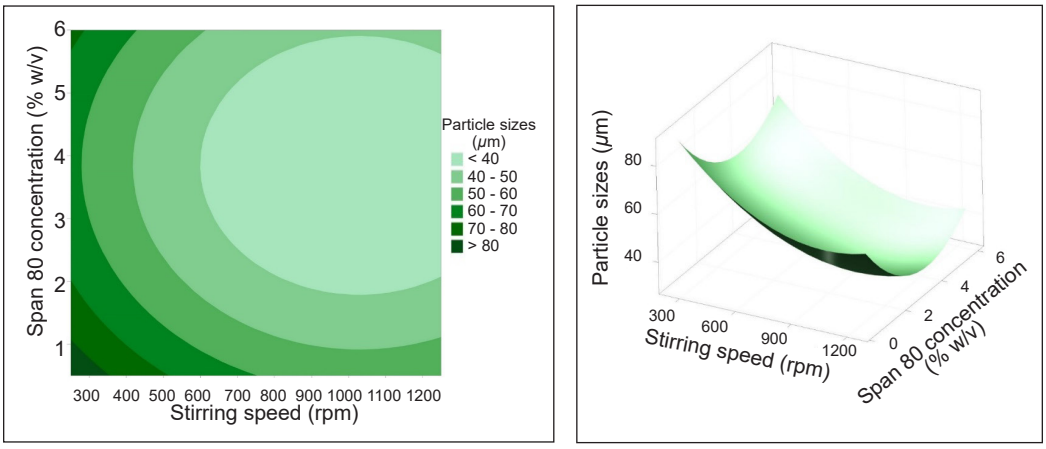

(a) (b)

Figure 2. The effects of stirring speed and Span 80 concentration on the mean particle sizes of μCBs: (a) contour; and (b) surface plots (With 3% w/v cellulose concentration; 65°C)

The effects of stirring speed and cellulose concentration on the mean particle sizes of the μCBs are shown in Figures 3(a) and (b). The results showed that the mean particle size would decrease using a lower stirring speed and higher cellulose concentration. The plots estimated a minimum of 15.3 µm cellulose beads would be obtained at 1031.4 rpm and 1.0% w/v of cellulose concentration. Conversely, the maximum mean particle size of 73.8 µm would be expected to be produced using a stirring speed at 251 rpm and 5.0% w/v cellulose concentration. The smallest particle size achieved experimentally was approximately 14.5 µm and the largest at around 42.3 µm when cellulose concentration increased from 1.0% w/v to 5% w/v, under 1000 rpm (Voon et al., 2017a).

The viscosity of the cellulose solution is dependent on the cellulose concentrations. An adequate viscosity can be found in a higher concentration of cellulose, which helps to resist the increased deformation forces (Schroeter et al., 2021). The number of cellulose molecules would increase when cellulose concentration increased (Chin et al., 2016). A slower agitation speed was accompanied during the process. It could lead to the formation of many big aggregates accompanied by high strength and resistance to the disintegration of porous structures (Li et al., 2022). Similarly, Druel et al. (2018) reported cellulose concentration as the major contributor to regulating the size of the beads. High cellulose concentration with low stirring speed would promote larger growth of particles, while low cellulose concentration with high stirring speed produced smaller particles. Previous studies highlighted the emulsification process of cellulose, enabling extensive production of microspheres with tailored particle sizes as well as distributions (Costa et al., 2019; Shi et al., 2021; Winuprasith & Suphantharika, 2015). Hence, the experimental results concurred with the predicted RSM data of approximately 15 µm and 70 µm with respect to the minimum and maximum particle sizes of the μCBs.

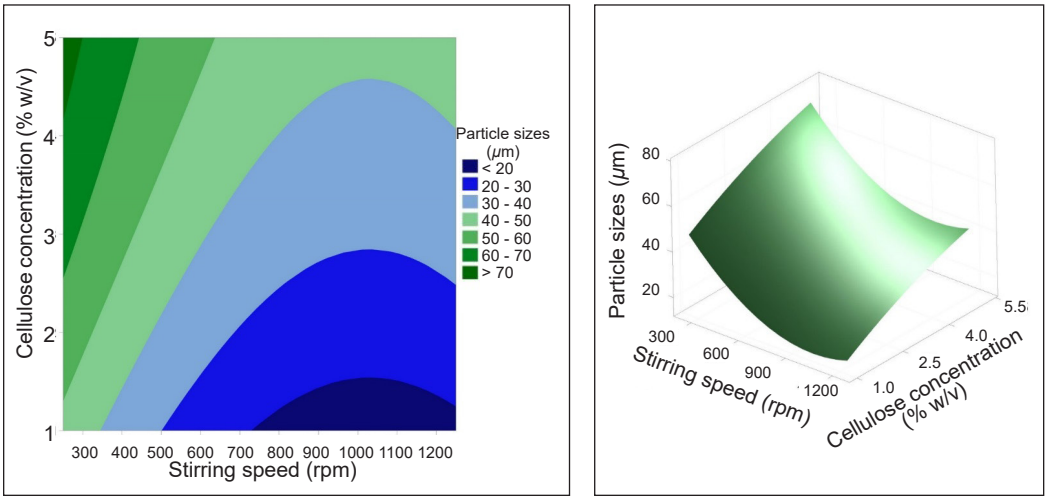

(a) (b)

Figure 3. The effects of stirring speed and cellulose concentration on the mean particle sizes of μCBs: (a) contour; and (b) surface plots (With 3.25% w/v Span 80 concentration; 65°C)

The contour and surface plots for the effects of stirring speed and reaction temperature on the mean particle sizes of μCBs were presented in Figures 4(a) and (b), respectively. The prediction of the plots for the minimum of 23.3 µm cellulose beads would require 1022 rpm and 34.2°C. When the reaction temperature increased to 100°C and with stirring speed at 251 rpm, a maximum mean particle size of 91 µm could be synthesized. It showed that the higher the stirring speed and the lower the reaction temperature, the smaller the

particle size of cellulose beads. Under an optimum 1000 rpm, the smallest 26.1 µm and the largest 67.2 µm of μCBs were obtained experimentally when the reaction temperature was at 30°C and 100°C, respectively (Voon et al., 2017a).

As previously stated, a low stirring speed can give rise to the agglomeration of particles. Temperature also had strong influential effects on particle sizes. Increased temperature is capable of speeding up the movement of droplets, increasing the instability of the oil/water interface, elevating the coalescence of the droplets, and eventually, causing phase separation of the emulsions (Tong et al., 2015). It was reported that an increase in temperature could decrease the viscosity of cellulose solution (Bhardwaj et al., 2018). Bigger particle size could be obtained due to decreasing viscosity and increased surface tension when the temperature of the cellulose solution increased (An et al., 2021). At a low temperature, coagulation took place at the inner layer as it enfolded the cellulose molecules densely and caused a little shrinkage of the bead (Trygg et al., 2013). The microemulsion droplets would remain stable under a low temperature and vice versa at higher temperatures, resulting in smaller beads. At the same time, an optimum stirring speed would also be required. Emulsion stability is also associated with the surfactant type and amount (Akbari & Nour, 2018). In addition, Span 80 surfactants are shown to be influenced by temperature due to the critical micelle concentration, whereby droplet size would remain the same above the critical value (Michor & Berg, 2015). Thus, an optimum temperature is critical to achieving the desired particle sizes of cellulose beads. Overall, the estimated RSM data agrees with the experimental work reported (Voon et al., 2017a).

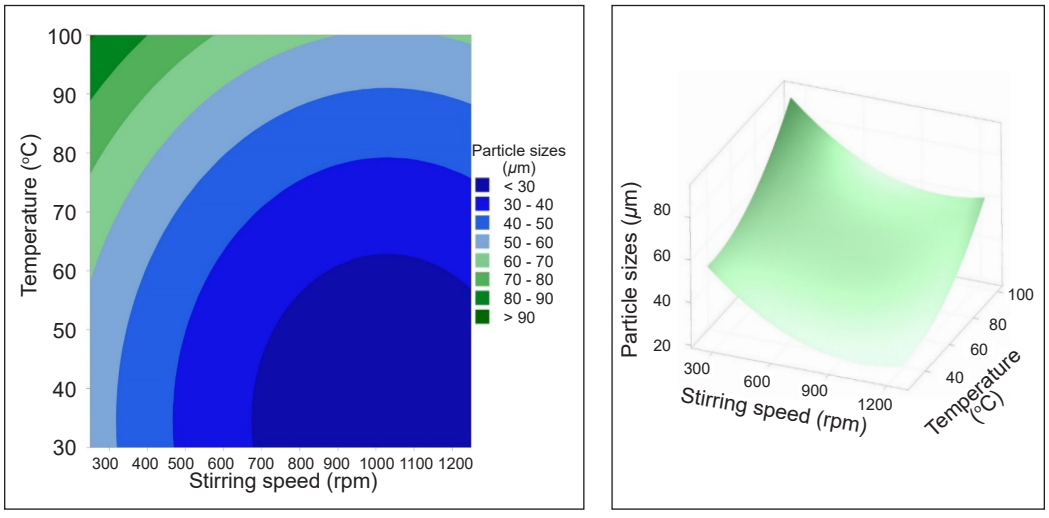

(a) (b)

Figure 4. The effects of stirring speed and temperature on the mean particle sizes of μCBs: (a) contour; and (b) surface plots (3% w/v cellulose concentration; 3.25% w/v Span 80 concentration)

Effects of Synthesis Parameters on the Particle Sizes of *n*CBs

Effect of Cellulose Concentration. Figures 5(a) and (b) showed the contour and surface plots of cellulose concentration on the mean particle sizes of *n*CBs. The plots showed that the mean particle sizes of *n*CBs increased linearly with the volume and concentration of the cellulose solution used in the synthesis. The plots predicted that a minimum of 0.01 nm could be obtained when 0.2 mL of 0.2% w/v cellulose concentration was used. On the other hand, a maximum of 200 nm of *n*CBs could be produced by using 1.0 mL of 1.0% w/v cellulose concentration. As determined experimentally, the smallest 57 nm and largest 200 nm of mean particle sizes of *n*CBs were obtained at 0.1% w/v and 1.0% w/v of cellulose concentration, respectively, using a constant 1.0 mL cellulose solution (Voon et al., 2017a).

The hydrophilicity of cellulose molecules can cause the aggregation of particles via hydrogen bonds and, eventually, the formation of bigger clusters of particles (Ren et al., 2014). Higher cellulose concentration will lead to high viscosity, creating a more firm network (Li et al., 2015). Interaction of cellulose/non-solvent molecules would increase under higher cellulose concentration, causing cellulose accumulation (Chin et al., 2016). Lince et al. (2008) reported the three stages of the formation of nanoparticles using nanoprecipitation: nucleation, growth, and aggregation. The insolubility of cellulose in water prompted nucleation to happen and form a solid nucleus within the drop. The deposition of more molecules will lead the nucleus to develop as mediated via coalescence as well as interchange with other drops (Ethayaraja et al., 2007). Ostwald ripening effect could cause the formation of large agglomerated particles over time (Maity et al., 2008).

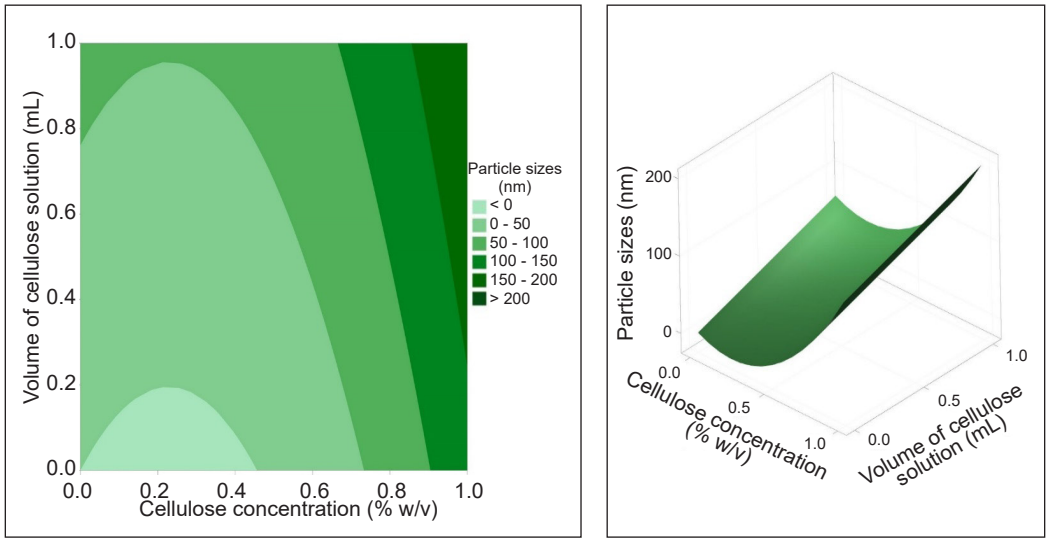

(a) (b)

Figure 5. The effects of cellulose concentration on the mean particle sizes of *n*CBs: (a) contour; and (b) surface plots

Hence, bigger *n*CBs would be expected to be produced when more volume of higher cellulose concentration was used, which further verified the consistency of the predicted RSM values with our previous work.

CONCLUSION

The synthesis parameters of μCBs and *n*CBs were successfully determined using response surface methodology via the central composite design. The effects of several important synthesis parameters such as the stirring speed (250–1250 rpm), Span 80 concentration (0.5–6.0% w/v), cellulose concentration (1–5% w/v) and the reaction temperature (30–100°C) on the mean particle sizes of μCBs were determined, whereas the volume (1 mL) and the concentration (0.1–1.0% w/v) of the cellulose solution were used to tailor the particle sizes of the *n*CBs. The results of this study would allow the control of μCBs and *n*CBs particle sizes via fine-tuning of the synthesis parameters. The model was proven capable of precisely elucidating the experimental data by manipulating the ANOVA, p-value, R^2, and adjusted R^2. Hence, this study demonstrated that by precisely controlling the synthesis parameters to modulate the particle sizes of the μCBs and *n*CBs. μCBs and *n*CBs with tailored particle sizes would have promising potential as controlled release carriers for drugs or fertilizers in various fields such as biomedical, pharmaceutical, and agricultural.

ACKNOWLEDGEMENTS

The authors wish to acknowledge the financial support rendered by Kementerian Pengajian Tinggi Malaysia (Malaysian Ministry of Higher Education) via the award of the Fundamental Research Grant Scheme (Grant No. FRGS/1/2020/STG05/UNIMAS/02/1).

REFERENCES

Akbari, S., & Nour, A. H. (2018). Emulsion types, stability mechanisms and rheology: A review. *International Journal of Innovative Research and Scientific Studies, 1*(1), 11-17. https://doi.org/10.53894/ijirss.v1i1.4

Alazab, A. A., & Saleh, T. A. (2022). Magnetic hydrophobic cellulose-modified polyurethane filter for efficient oil-water separation in a complex water environment. *Journal of Water Process Engineering, 50*, Article 103125. https://doi.org/10.1016/j.jwpe.2022.103125

Allouss, D., Essamlali, Y., Amadine, O., Chakir, A., & Zahouily, M. (2019). Response surface methodology for optimization of methylene blue adsorption onto carboxymethyl cellulose-based hydrogel beads: Adsorption kinetics, isotherm, thermodynamics and reusability studies. *RSC Advances, 9*(65), 37858-37869. https://doi.org/10.1039/c9ra06450h

Alnaief, M., Alzaitoun, M. A., García-González, C. A., & Smirnova, I. (2011). Preparation of biodegradable nanoporous microspherical aerogel based on alginate. *Carbohydrate Polymers, 84*(3), 1011-1018. https://doi.org/10.1016/j.carbpol.2010.12.060

An, H. J., Park, H., & Cho, B. U. (2021). Effect of temperature of tetraethylammonium hydroxide/urea/cellulose solution on surface tension and cellulose bead size. *Journal of Korea Technical Association of the Pulp and Paper Industry, 53*(6), 69-76. https://doi.org/10.7584/jktappi.2021.12.53.6.69

Balart, R., Garcia-Garcia, D., Fombuena, V., Quiles-Carrillo, L., & Arrieta, M. P. (2021). Biopolymers from natural resources. *Polymers, 13*(15), Article 2532. https://doi.org/10.3390/polym13152532

Bhardwaj, P., Kamil, M., & Panda, M. (2018). Surfactant-polymer interaction: effect of hydroxypropylmethyl cellulose on the surface and solution properties of gemini surfactants. *Colloid and Polymer Science, 296*(11), 1879-1889. https://doi.org/10.1007/s00396-018-4409-5

Califano, D., Patenall, B. L., Kadowaki, M. A. S., Mattia, D., Scott, J. L., & Edler, K. J. (2021). Enzyme-functionalized cellulose beads as a promising antimicrobial material. *Biomacromolecules, 22*(2), 754-762. https://doi.org/10.1021/acs.biomac.0c01536

Carvalho, J. P. F., Silva, A. C. Q., Silvestre, A. J. D., Freire, C. S. R., & Vilela, C. (2021). Spherical cellulose micro and nanoparticles: A review of recent developments and applications. *Nanomaterials, 11*(10), Article 2744. https://doi.org/10.3390/nano11102744

Chin, S. F., Jimmy, F. B., & Pang, S. C. (2016). Fabrication of cellulose aerogel from sugarcane bagasse as drug delivery carriers. *Journal of Physical Science, 27*(3), 159-168. https://doi.org/10.21315/jps2016.27.3.10

Chin, S. F., Azman, A., & Pang, S. C. (2014). Size controlled synthesis of starch nanoparticles by a microemulsion method. *Journal of Nanomaterials, 2014*, Article 763736. https://doi.org/10.1155/2014/763736

Chin, S. F., Jimmy, F. B., & Pang, S. C. (2018). Size controlled fabrication of cellulose nanoparticles for drug delivery applications. *Journal of Drug Delivery Science and Technology, 43*, 262-266. https://doi.org/10.1016/j.jddst.2017.10.021

Chin, S. F., Jong, S. J., & Yeo, Y. J. (2021). Optimization of cellulose-based hydrogel synthesis using response surface methodology. *Biointerface Research in Applied Chemistry, 12*(6), 7136-7146. https://doi.org/10.33263/BRIAC126.71367146

Chin, S. F., Yazid, S. N. A. M., & Pang, S. C. (2014). Preparation and characterization of starch nanoparticles for controlled release of curcumin. *International Journal of Polymer Science, 2014*, Article 340121. https://doi.org/10.1155/2014/340121

Ching, Y. C., Gunathilake, T. M. S. U., Chuah, C. H., Ching, K. Y., Singh, R., & Liou, N. S. (2019). Curcumin/tween 20-incorporated cellulose nanoparticles with enhanced curcumin solubility for nano-drug delivery: Characterization and in vitro evaluation. *Cellulose, 26*(9), 5467-5481. https://doi.org/10.1007/s10570-019-02445-6

Conforti, C., Giuffrida, R., Fadda, S., Fai, A., Romita, P., Zalaudek, I., & Dianzani, C. (2021). Topical dermocosmetics and acne vulgaris. *Dermatologic Therapy, 34*(1), Article e14436. https://doi.org/10.1111/dth.14436

Costa, C., Medronho, B., Filipe, A., Mira, I., Lindman, B., Edlund, H., & Norgren, M. (2019). Emulsion formation and stabilization by biomolecules: The leading role of cellulose. *Polymers, 11*(10), Article 1570. https://doi.org/10.3390/polym11101570

Culica, M. E., Chibac-Scutaru, A. L., Mohan, T., & Coseri, S. (2021). Cellulose-based biogenic supports, remarkably friendly biomaterials for proteins and biomolecules. *Biosensors and Bioelectronics, 182*, Article 113170. https://doi.org/10.1016/j.bios.2021.113170

Druel, L., Niemeyer, P., Milow, B., & Budtova, T. (2018). Rheology of cellulose-[DBNH][CO2Et] solutions and shaping into aerogel beads. *Green Chemistry, 20*(17), 3993-4002. https://doi.org/10.1039/c8gc01189c

Du, K., Li, S., Zhao, L., Qiao, L., Ai, H., & Liu, X. (2018). One-step growth of porous cellulose beads directly on bamboo fibers via oxidation-derived method in aqueous phase and their potential for heavy metal ions adsorption. *ACS Sustainable Chemistry and Engineering, 6*(12), 17068-17075. https://doi.org/10.1021/acssuschemeng.8b04433

Essawy, H. A., Ghazy, M. B. M., El-Hai, F. A., & Mohamed, M. F. (2016). Superabsorbent hydrogels via graft polymerization of acrylic acid from chitosan-cellulose hybrid and their potential in controlled release of soil nutrients. *International Journal of Biological Macromolecules, 89*, 144-151. https://doi.org/10.1016/j.ijbiomac.2016.04.071

Ethayaraja, M., Ravikumar, C., Muthukumaran, D., Dutta, K., & Bandyopadhyaya, R. (2007). CdS−ZnS core−shell nanoparticle formation: Experiment, mechanism, and simulation. *The Journal of Physical Chemistry C, 111*(8), 3246-3252. https://doi.org/10.1021/jp066066j

França, D., de Barros, J. R. S., & Faez, R. (2021). Spray-dried cellulose nanofibrils microparticles as a vehicle for enhanced efficiency fertilizers. *Cellulose, 28*(3), 1571-1585. https://doi.org/10.1007/s10570-020-03609-5

Gericke, M., Trygg, J., & Fardim, P. (2013). Functional cellulose beads: Preparation, characterization, and applications. *Chemical Reviews, 113*(7), 4812-4836. https://doi.org/10.1021/cr300242j

Gomes, M. H. F., Callaghan, C., Mendes, A. C. S., Edler, K. J., Mattia, D., de Jong van Lier, Q., & de Carvalho, H. W. P. (2022). Cellulose microbeads: Toward the controlled release of nutrients to plants. *ACS Agricultural Science & Technology, 2*(2), 340-348. https://doi.org/10.1021/acsagscitech.1c00233

Guan, H., Li, J., Zhang, B., & Yu, X. (2017). Synthesis, properties, and humidity resistance enhancement of biodegradable cellulose-containing superabsorbent polymer. *Journal of Polymers, 2017*, Article 3134681. https://doi.org/10.1155/2017/3134681

Gülsu, A., & Yüksektepe, E. (2021). Preparation of spherical cellulose nanoparticles from recycled waste cotton for anticancer drug delivery. *Chemistry Select, 6*(22), 5419-5425. https://doi.org/10.1002/slct.202101683

Guo, H., Lei, B., Yu, J., Chen, Y., & Qian, J. (2021). Immobilization of lipase by dialdehyde cellulose crosslinked magnetic nanoparticles. *International Journal of Biological Macromolecules, 185*, 287-296. https://doi.org/10.1016/j.ijbiomac.2021.06.073

Hakim, S. L., Kusumasari, F. C., & Budianto, E. (2020). Optimization of biodegradable PLA/PCL microspheres preparation as controlled drug delivery carrier. *Materials Today: Proceedings, 22*, 306-313. https://doi.org/10.1016/j.matpr.2019.08.156

Hamidon, T. S., Adnan, R., Haafiz, M. K. M., & Hussin, M. H. (2022). Cellulose-based beads for the adsorptive removal of wastewater effluents: A review. *Environmental Chemistry Letters, 20*(3), 1965-2017. https://doi.org/10.1007/s10311-022-01401-4

Harada, N., Nakamura, J., & Uyama, H. (2021). Single-step fabrication and environmental applications of activated carbon-containing porous cellulose beads. *Reactive and Functional Polymers*, *160*, Article 104830. https://doi.org/10.1016/j.reactfunctpolym.2021.104830

Ho, B. K., Chin, S. F., & Pang, S. C. (2020). pH-responsive carboxylic cellulose acetate nanoparticles for controlled release of penicillin G. *Journal of Science: Advanced Materials and Devices, 5*(2), 224-232. https://doi.org/10.1016/j.jsamd.2020.04.002

Hu, Z. H., Omer, A. M., Ouyang, X. K., & Yu, D. (2018). Fabrication of carboxylated cellulose nanocrystal/sodium alginate hydrogel beads for adsorption of Pb(II) from aqueous solution. *International Journal of Biological Macromolecules, 108*, 149-157. https://doi.org/10.1016/j.ijbiomac.2017.11.171

Jampi, A. L. W., Chin, S. F., Wasli, M. E., & Chia, C. H. (2021). Preparation of cellulose hydrogel from sago pith waste as a medium for seed germination. *Journal of Physical Science, 32*(1), 13-26. https://doi.org/10.21315/JPS2021.32.1.2

Jancy, S., Shruthy, R., & Preetha, R. (2020). Fabrication of packaging film reinforced with cellulose nanoparticles synthesised from jack fruit non-edible part using response surface methodology. *International Journal of Biological Macromolecules*, *142,* 63-72. https://doi.org/10.1016/j.ijbiomac.2019.09.066

Jo, S., Park, S., Oh, Y., Hong, J., Kim, H. J., Kim, K. J., Oh, K. K., & Lee, S. H. (2019). Development of cellulose hydrogel microspheres for lipase immobilization. *Biotechnology and Bioprocess Engineering, 24*(1), 145-154. https://doi.org/10.1007/s12257-018-0335-0

Kalia, S., Dufresne, A., Cherian, B. M., Kaith, B. S., Avérous, L., Njuguna, J., & Nassiopoulos, E. (2011). Cellulose-based bio- and nanocomposites: A review. *International Journal of Polymer Science, 2011*, 1-35. https://doi.org/10.1155/2011/837875

Karri, R. R., Tanzifi, M., Yaraki, M. T., & Sahu, J. N. (2018). Optimization and modeling of methyl orange adsorption onto polyaniline nano-adsorbent through response surface methodology and differential evolution embedded neural network. *Journal of Environmental Management, 223*, 517-529. https://doi.org/10.1016/j.jenvman.2018.06.027

Kemin, L. V., & Chin, S. F. (2020). Amino-starch nanoparticles as controlled release nanocarriers for curcumin. *Journal of Physical Science, 31*(2), 1-14. https://doi.org/10.21315/jps2020.31.2.1

Kim, B., Choi, Y., Choi, J., Shin, Y., & Lee, S. (2020). Effect of surfactant on wetting due to fouling in membrane distillation membrane: Application of response surface methodology (RSM) and artificial neural networks (ANN). *Korean Journal of Chemical Engineering, 37*(1), 1-10. https://doi.org/10.1007/s11814-019-0420-x

Lechuga, M., Fernández-Serrano, M., Jurado, E., Núñez-Olea, J., & Ríos, F. (2016). Acute toxicity of anionic and non-ionic surfactants to aquatic organisms. *Ecotoxicology and Environmental Safety, 125*, 1-8. https://doi.org/10.1016/j.ecoenv.2015.11.027

Lee, J., & Patel, R. (2022). Wastewater treatment by polymeric microspheres: A review. *Polymers*, *14*(9), Article 1890. https://doi.org/10.3390/polym14091890

Lefroy, K. S., Murray, B. S., & Ries, M. E. (2022). Relationship between size and cellulose content of cellulose microgels (CMGs) and their water-in-oil emulsifying capacity. *Colloids and Surfaces A: Physicochemical and Engineering Aspects, 647*, Article 128926. https://doi.org/10.1016/j.colsurfa.2022.128926

Li, H., Kruteva, M., Dulle, M., Wang, Z., Mystek, K., Ji, W., Pettersson, T., & Wågberg, L. (2022). Understanding the drying behavior of regenerated cellulose gel beads: The effects of concentration and nonsolvents. *ACS Nano, 16*(2), 2608-2620. https://doi.org/10.1021/acsnano.1c09338

Li, M. C., Wu, Q., Song, K., Lee, S., Qing, Y., & Wu, Y. (2015). Cellulose nanoparticles: Structure-morphology-rheology relationships. *ACS Sustainable Chemistry and Engineering, 3*(5), 821-832. https://doi.org/https://doi.org/10.1021/acssuschemeng.5b00144

Li, M., Zhang, H., Wu, Z., Zhu, Z., & Jia, X. (2022). DPD simulation on the transformation and stability of O/W and W/O microemulsions. *Molecules, 27*(4), Article 1361. https://doi.org/10.3390/molecules27041361

Li, Q., Dang, L., Li, S., Liu, X., Guo, Y., Lu, C., Kou, X., & Wang, Z. (2018). Preparation of α-linolenic-acid-loaded water-in-oil-in-water microemulsion and its potential as a fluorescent delivery carrier with a free label. *Journal of Agricultural and Food Chemistry, 66*(49), 13020-13030. https://doi.org/10.1021/acs.jafc.8b04678

Li, Z., Wu, W., Jiang, W., Zhang, L., Li, Y., Tan, Y., Chen, S., Lv, M., Luo, F., Luo, T., & Wei, G. (2020). Preparation and regeneration of a thermo-sensitive adsorbent material: Methyl cellulose/calcium alginate beads (MC/CABs). *Polymer Bulletin, 77*(4), 1707-1728. https://doi.org/10.1007/s00289-019-02808-w

Lince, F., Marchisio, D. L., & Barresi, A. A. (2008). Strategies to control the particle size distribution of poly-ε-caprolactone nanoparticles for pharmaceutical applications. *Journal of Colloid and Interface Science, 322*(2), 505-515. https://doi.org/10.1016/j.jcis.2008.03.033

Liu, Y., Qiao, L., Wang, A., Li, Y., Zhao, L., & Du, K. (2021). Tentacle-type poly(hydroxamic acid)-modified macroporous cellulose beads: Synthesis, characterization, and application for heavy metal ions adsorption. *Journal of Chromatography A, 1645*, Article 462098. https://doi.org/10.1016/j.chroma.2021.462098

Luo, X., & Zhang, L. (2010). Creation of regenerated cellulose microspheres with diameter ranging from micron to millimeter for chromatography applications. *Journal of Chromatography A, 1217*(38), 5922-5929. https://doi.org/10.1016/j.chroma.2010.07.026

Machado, T. O., Grabow, J., Sayer, C., de Araújo, P. H. H., Ehrenhard, M. L., & Wurm, F. R. (2022). Biopolymer-based nanocarriers for sustained release of agrochemicals: A review on materials and social science perspectives for a sustainable future of agri- and horticulture. *Advances in Colloid and Interface Science, 303*, Article 102645. https://doi.org/10.1016/j.cis.2022.102645

Maity, D., Ding, J., & Xue, J. M. (2008). Synthesis of magnetite nanoparticles by thermal decomposition: Time, temperature, surfactant and solvent effects. *Functional Materials Letters, 1*(3), 189-193. https://doi.org/10.1142/S1793604708000381

Meng, R., Liu, L., Jin, Y., Luo, Z., Gao, H., & Yao, J. (2019). Recyclable carboxylated cellulose beads with tunable pore structure and size for highly efficient dye removal. *Cellulose, 26*(17), 8963-8969. https://doi.org/10.1007/s10570-019-02733-1

Michor, E. L., & Berg, J. C. (2015). Temperature effects on micelle formation and particle charging with span surfactants in apolar media. *Langmuir, 31*(35), 9602-9607. https://doi.org/10.1021/acs.langmuir.5b02711

Mohan, T., Ajdnik, U., Nagaraj, C., Lackner, F., Štiglic, A. D., Palani, T., Amornkitbamrung, L., Gradišnik, L., Maver, U., Kargl, R., & Kleinschek, K. S. (2022). One-step fabrication of hollow spherical cellulose

beads: Application in pH-responsive therapeutic delivery. *ACS Applied Materials and Interfaces, 14*(3), 3726-3739. https://doi.org/10.1021/acsami.1c19577

Pal, N., Agarwal, M., & Gupta, R. (2022). Green synthesis of guar gum/Ag nanoparticles and their role in peel-off gel for enhanced antibacterial efficiency and optimization using RSM. *International Journal of Biological Macromolecules, 221*, 665-678. https://doi.org/10.1016/j.ijbiomac.2022.09.036

Pang, S. C., Chin, S. F., & Yih, V. (2011). Conversion of cellulosic waste materials into nanostructured ceramics and nanocomposites. *Advanced Materials Letters, 2*(2), 118-124. https://doi.org/10.5185/amlett.2011.1203

Pang, S. C., Voon, L. K., & Chin, S. F. (2018). Controlled depolymerization of cellulose fibres isolated from lignocellulosic biomass wastes. *International Journal of Polymer Science, 2018*, 1-11. https://doi.org/10.1155/2018/6872893

Ren, S., Sun, X., Lei, T., & Wu, Q. (2014). The effect of chemical and high-pressure homogenization treatment conditions on the morphology of cellulose nanoparticles. *Journal of Nanomaterials, 2014,* 168-168. https://doi.org/10.1155/2014/582913

Roque, L., Fernández, M., Benito, J. M., & Escudero, I. (2020). Stability and characterization studies of Span 80 niosomes modified with CTAB in the presence of NaCl. *Colloids and Surfaces A: Physicochemical and Engineering Aspects, 601*, Article 124999. https://doi.org/10.1016/j.colsurfa.2020.124999

Russell-Jones, G., & Himes, R. (2011). Water-in-oil microemulsions for effective transdermal delivery of proteins. *Expert Opinion on Drug Delivery, 8*(4), 537-546. https://doi.org/10.1517/17425247.2011.559458

Saleh, T. A. (2021). Protocols for synthesis of nanomaterials, polymers, and green materials as adsorbents for water treatment technologies. *Environmental Technology and Innovation, 24*, Article 101821. https://doi.org/10.1016/j.eti.2021.101821

Schroeter, B., Yonkova, V. P., Niemeyer, N. A. M., Jung, I., Preibisch, I., Gurikov, P., & Smirnova, I. (2021). Cellulose aerogel particles: Control of particle and textural properties in jet cutting process. *Cellulose, 28*(1), 223-239. https://doi.org/10.1007/s10570-020-03555-2

Sebeia, N., Jabli, M., Ghanmi, H., Ghith, A., & Saleh, T. A. (2021). Effective dyeing of cotton fibers using cynomorium coccineum L. peel extracts: Study of the influential factors using surface response methodology. *Journal of Natural Fibers, 18*(1), 21-33. https://doi.org/10.1080/15440478.2019.1612302

Shahnaz, T., Sharma, V., Subbiah, S., & Narayanasamy, S. (2020). Multivariate optimisation of Cr(VI), Co(III) and Cu(II) adsorption onto nanobentonite incorporated nanocellulose/chitosan aerogel using response surface methodology. *Journal of Water Process Engineering, 36*, Article 101283. https://doi.org/10.1016/j.jwpe.2020.101283

Shi, F., Lin, D. Q., Phottraithip, W., & Yao, S. J. (2011). Preparation of cellulose-tungsten carbide composite beads with ionic liquid for expanded bed application. *Journal of Applied Polymer Science, 119*(6), 3453-3461. https://doi.org/10.1002/app.33005

Shi, W., Ching, Y. C., & Chuah, C. H. (2021). Preparation of aerogel beads and microspheres based on chitosan and cellulose for drug delivery: A review. *International Journal of Biological Macromolecules, 170*, 751-767. https://doi.org/10.1016/j.ijbiomac.2020.12.214

Song, M., Liu, W., Wang, Q., Wang, J., & Chai, J. (2020). A surfactant-free microemulsion containing diethyl malonate, ethanol, and water: Microstructure, micropolarity and solubilizations. *Journal of Industrial and Engineering Chemistry, 83*, 81-89. https://doi.org/10.1016/j.jiec.2019.11.016

Tay, S. H., Pang, S. C., & Chin, S. F. (2012). A facile approach for controlled synthesis of hydrophilic starch-based nanoparticles from native sago starch. *Starch/Staerke, 64*(12), 984-990. https://doi.org/10.1002/star.201200056

Tong, K., Zhao, C., Sun, Z., & Sun, D. (2015). Formation of concentrated nanoemulsion by W/O microemulsion dilution method: Biodiesel, tween 80, and water system. *ACS Sustainable Chemistry & Engineering, 3*(12), 3299-3306. https://doi.org/10.1021/acssuschemeng.5b00903

Trygg, J., Fardim, P., Gericke, M., Mäkilä, E., & Salonen, J. (2013). Physicochemical design of the morphology and ultrastructure of cellulose beads. *Carbohydrate Polymers, 93*(1), 291-299. https://doi.org/10.1016/j.carbpol.2012.03.085

Voon, L. K., Pang, S. C., & Chin, S. F. (2015). Highly porous cellulose beads of controllable sizes derived from regenerated cellulose of printed paper wastes. *Materials Letters, 164*, 264-266. https://doi.org/10.1016/j.matlet.2015.10.161

Voon, L. K., Pang, S. C., & Chin, S. F. (2016). Regeneration of cello-oligomers via selective depolymerization of cellulose fibers derived from printed paper wastes. *Carbohydrate Polymers, 142*, 31-37. https://doi.org/10.1016/j.carbpol.2016.01.027

Voon, L. K., Pang, S. C., & Chin, S. F. (2017a). Optimizing delivery characteristics of curcumin as a model drug via tailoring mean diameter ranges of cellulose beads. *International Journal of Polymer Science, 2017*, Article 2581767. https://doi.org/10.1155/2017/2581767

Voon, L. K., Pang, S. C., & Chin, S. F. (2017b). Porous cellulose beads fabricated from regenerated cellulose as potential drug delivery carriers. *Journal of Chemistry, 2017*, Article 1943432. https://doi.org/10.1155/2017/1943432

Wang, G., Yang, X., & Wang, W. (2019). Reinforcing linear low-density polyethylene with surfactant-treated microfibrillated cellulose. *Polymers, 11*(3), Article 441. https://doi.org/10.3390/polym11030441

Winuprasith, T., & Suphantharika, M. (2015). Properties and stability of oil-in-water emulsions stabilized by microfibrillated cellulose from mangosteen rind. *Food Hydrocolloids, 43*, 690-699. https://doi.org/10.1016/j.foodhyd.2014.07.027

Wu, R., & Hu, C. (2021). Fabrication of magnetic cellulose microspheres by response surface methodology and adsorption study for Cu(II). *Cellulose, 28*(3), 1499-1511. https://doi.org/10.1007/s10570-020-03640-6

Xu, F., & Cho, B. U. (2022). Preparation of porous regenerated cellulose microstructures via emulsion-coagulation technique. *Cellulose, 29*(3), 1527-1542. https://doi.org/10.1007/s10570-022-04428-6

Yan, X., Bernard, J., & Ganachaud, F. (2021). Nanoprecipitation as a simple and straightforward process to create complex polymeric colloidal morphologies. *Advances in Colloid and Interface Science, 294*, Article 102474. https://doi.org/10.1016/j.cis.2021.102474